Supplementary Materials for

Alleviation of liver fibrosis by inhibiting a non-canonical ATF4-regulated enhancer program in hepatic stellate cells

Authors: Li-Xian Yang[1,2,3†], Chuangye Qi[4†], Si Lu[1,5†], Xiang-Shi Ye[1,2†], Parnaz Merikhian[4,6], Du-Yu Zhang[1,2], Tao Yao[1,2,7], Jiang-Sha Zhao[1,2], Ying Wu[7,8], Yongshi Jia[3], Bo Shan[1,2], Jinghai Chen[9], Xiaozhou Mou[10], Jia You[11*], Wenbo Li[4,6*], and Yu-Xiong Feng[1,2*]

Affiliations:

1. Zhejiang Key Laboratory of Pancreatic Disease, The First Affiliated Hospital, Zhejiang Key Laboratory of Frontier Medical Research on Cancer Metabolism, Institute of Translational Medicine, Zhejiang University School of Medicine, Hangzhou, China

2. Institute of Fundamental and Transdisciplinary Research, Cancer Center, Zhejiang University, Hangzhou, China

3. Cancer Center, Department of Radiation Oncology, Zhejiang Provincial People's Hospital, Affiliated People's Hospital, Hangzhou Medical College, Hangzhou, China.

4. Department of Biochemistry and Molecular Biology, McGovern Medical School, University of Texas Health Science Center, Houston, USA.

5. Department of Head and Neck Surgery, Sir Run-Run Shaw Hospital, Zhejiang University School of Medicine, Hangzhou, China.

6. Graduate School of Biomedical Sciences, University of Texas MD Anderson Cancer Center and UTHealth, Houston, USA.

7. College of Life Sciences, Zhejiang Chinese Medical University, Hangzhou, China.

8. Zhejiang Academy of Traditional Chinese Medicine, Tongde Hospital of Zhejiang Province, Hangzhou, China.

9. Department of Cardiology of Second Affiliated Hospital, State Key Laboratory of Transvascular Implantation Devices, Heart Regeneration and Repair Key Laboratory of Zhejiang Province, Institute of Translational Medicine, Zhejiang University School of Medicine, Hangzhou, China.

10. Clinical Research Institute, Zhejiang Provincial People's Hospital, People's Hospital of Hangzhou Medical College, Hangzhou, China.

11. School of Life Sciences, Westlake University, Hangzhou, China.

*Corresponding authors.

Email: yxfeng@zju.edu.cn (Yu-Xiong Feng), wenbo.li@uth.tmc.edu (Wenbo Li), and youjia@westlake.edu.cn (Jia You)

†These authors contributed equally to this work.

This PDF file includes:

Supplementary Fig. 1 ATF4 regulates classical stress response genes in ER stress or amino acid deprivation.

Supplementary Fig. 2 ATF4 positively regulates the EMT program in epithelial and mesenchymal cells.

Supplementary Fig. 3 Validation of depletion of ATF4 in the HSC-specific *Atf4* knockout mice.

Supplementary Fig. 4 The landscape of ATF4- and H3K27ac- binding regions in different conditions.

Supplementary Fig. 5 Pharmacological inhibition of eIF2α-ATF4 alleviates CCl_4-induced liver fibrosis.

Supplementary Fig. 6 Pharmacological inhibition of eIF2α-ATF4 alleviates BDL- or TAA-induced liver fibrosis.

Supplementary Fig. 7 Clinical relevance of HSC-ATF4 in human liver fibrosis.

Supplementary Table 1 Sequences of quantitative PCR primers.

Supplementary Table 2 Sequences of primers used for plasmid construction.

Supplementary Fig. 1

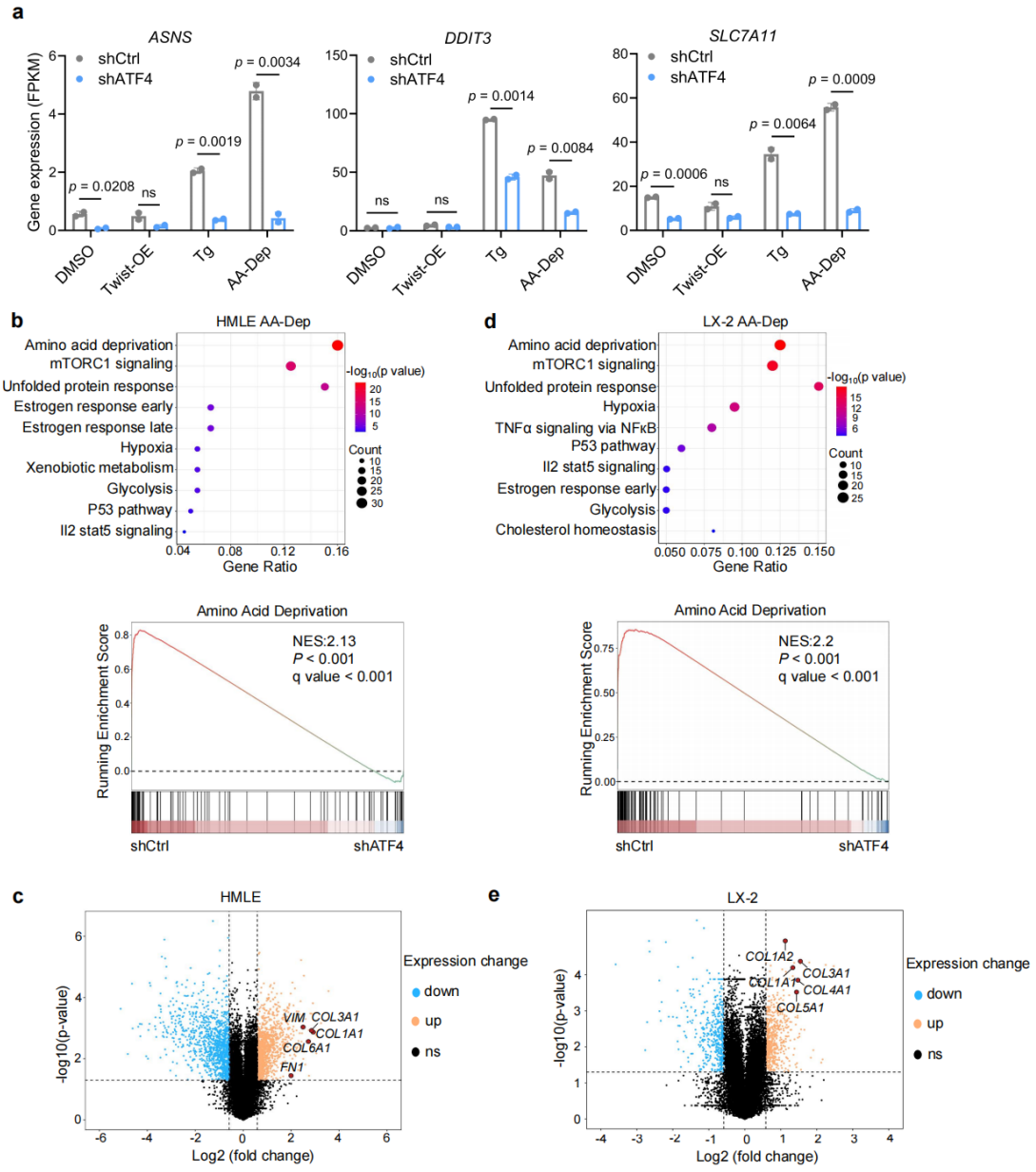

Supplementary Fig. 1 ATF4 regulates classical stress response genes in ER stress or amino acid deprivation. RNA-seq was conducted on the HMLE or LX-2 cells transduced with a scramble shRNA (shCtrl) or an ATF4-targeted shRNA (shATF4) and treated with indicated conditions (n = 2 biological replicates; Twist-OE, Twist overexpression; Tg, thapsigargin; AA-Dep, amino acid deprivation). **a,** The expression of stress response genes (*ASNS*, *DDIT3*, and *SLC7A11*) in different treatment conditions by bulk RNA-seq for HMLE cells. **b,** GO enrichment analysis for down-regulated genes by ATF4 knockdown under AA-Dep treatment in HMLE cells (upper panel). Hypergeometric test was used to identify significant enrichment pathways ($P < 0.01$). GSEA of amino acid deprivation in ATF4 knockdown compared with scramble (lower panel). The statistical significance (nominal *P* value) of the normalized enrichment score (NES) was generated by employing an empirical phenotype-based permutation test procedure. **c,** Volcano plot showing the differentially expressed genes (DEGs) in shCtrl HMLE cells compared with shATF4 under Twist-induction condition. Upregulated or downregulated genes are highlighted in orange or blue, respectively. The examples of significantly changed EMT genes, including *FN1*, *VIM*, *COL1A1*, *COL3A1*, and *COL6A1*, were labeled. **d,** GO enrichment analysis for down-regulated genes by ATF4 knockdown under AA-Dep treatment in LX-2 cells (upper panel). Hypergeometric test was used to identify significant enrichment pathways. GSEA of amino acid deprivation in ATF4 knockdown compared with scramble (lower panel). The statistical significance (nominal *P* value) of the normalized enrichment score (NES) was generated by employing an empirical phenotype-based permutation test procedure. **e,** Volcano plot showing the DEGs in shCtrl LX-2 cells compared with shATF4 LX-2 cells under TGFβ treatment. Upregulated or downregulated genes are highlighted in orange or blue, respectively. The examples of significantly changed EMT genes, including *COL1A1*, *COL1A2*, *COL3A1*, *COL4A1*, and *COL5A1* were labeled. Hypergeometric distribution tests were applied for GO enrichment analysis, and weighted Kolmogorov-Smirnov tests were applied for GSEA. These analyses were

conducted using the average data of two biological replicates. ***$p < 0.001$; **$p < 0.01$; *$p < 0.05$. Source data are provided as a Source Data file.

Supplementary Fig. 2

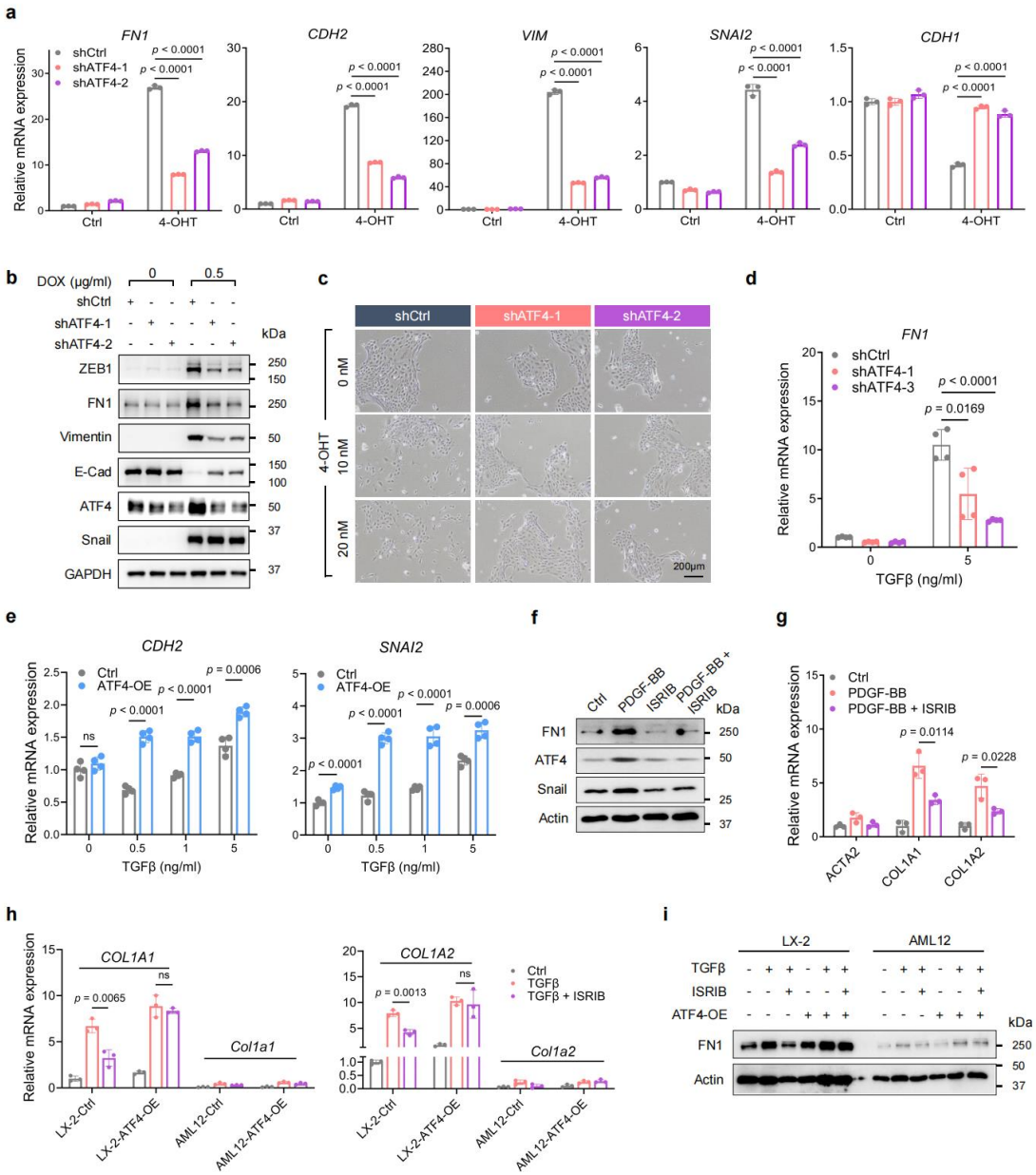

Supplementary Fig. 2 ATF4 positively regulates the EMT program in epithelial and mesenchymal cells. a, qPCR analysis of EMT marker genes mRNA expression in HMLE-shCtrl and HMLE-shATF4 cells treated with solvent control or 4-OHT (20nM) for 10 days (n = 3 biological replicates). **b,** Western blots showing the expression of EMT marker genes of HMLER-shCtrl and HMLER-shATF4 cells treated with doxycycline (DOX) for 4 days. DOX induces Snail overexpression. The experiment was repeated three times. **c,** The morphology and distribution of HMLE-shCtrl and HMLE-shATF4 cells treated with increasing concentrations of 4-OHT for 10 days. Representative phase-contrast microscope images were shown (derived from 3 biological replicates per group). **d,** qPCR analysis of EMT marker genes mRNA expression in LX-2-shCtrl and LX-2-shATF4 cells treated with TGFβ for 2 days (n = 4 biological replicates). **e,** qPCR analysis of mesenchymal marker genes mRNA expression in LX-2 cells overexpressing ATF4 treated with or without increasing concentrations of TGFβ (0, 0.5, 1, and 5 ng/ml) for 2 days (n = 4 biological replicates). **f,** Western blots showing the expression of fibrotic genes in LX-2 cells treated with solvent control, PDGF-BB, ISRIB, or combined PDGF-BB and ISRIB for two days. The experiment was repeated three times. **g,** qPCR analysis for collagen genes in LX-2 cells treated with solvent control, PDGF-BB, or combined PDGF-BB and ISRIB for two days (n = 3 biological replicates). **h,** qPCR analysis for collagen genes in LX-2 or AML12 cells overexpressing a control vector or an ATF4-expression construct, treated with or without TGFβ or TGFβ combined with ISRIB; the expression of collagen genes was normalized to the expression of GAPDH or Gapdh in LX-2 or AML12 cells, respectively (n = 3 biological replicates). **i,** Western blots showing the expression of FN1 in LX-2 or AML12 cells overexpressing a control vector or an ATF4-expression construct, treated with or without TGFβ or TGFβ combined with ISRIB. The experiment was repeated three times. Data are presented as mean ± s.e.m and representative of at least three independent experiments. Unpaired, two-tailed Student's t-tests were applied for **a, d, e, g, and h**. ****$p < 0.0001$; ***$p < 0.001$; **$p < 0.01$; *$p < 0.05$. Source data are provided as a Source Data file.

Supplementary Fig. 3

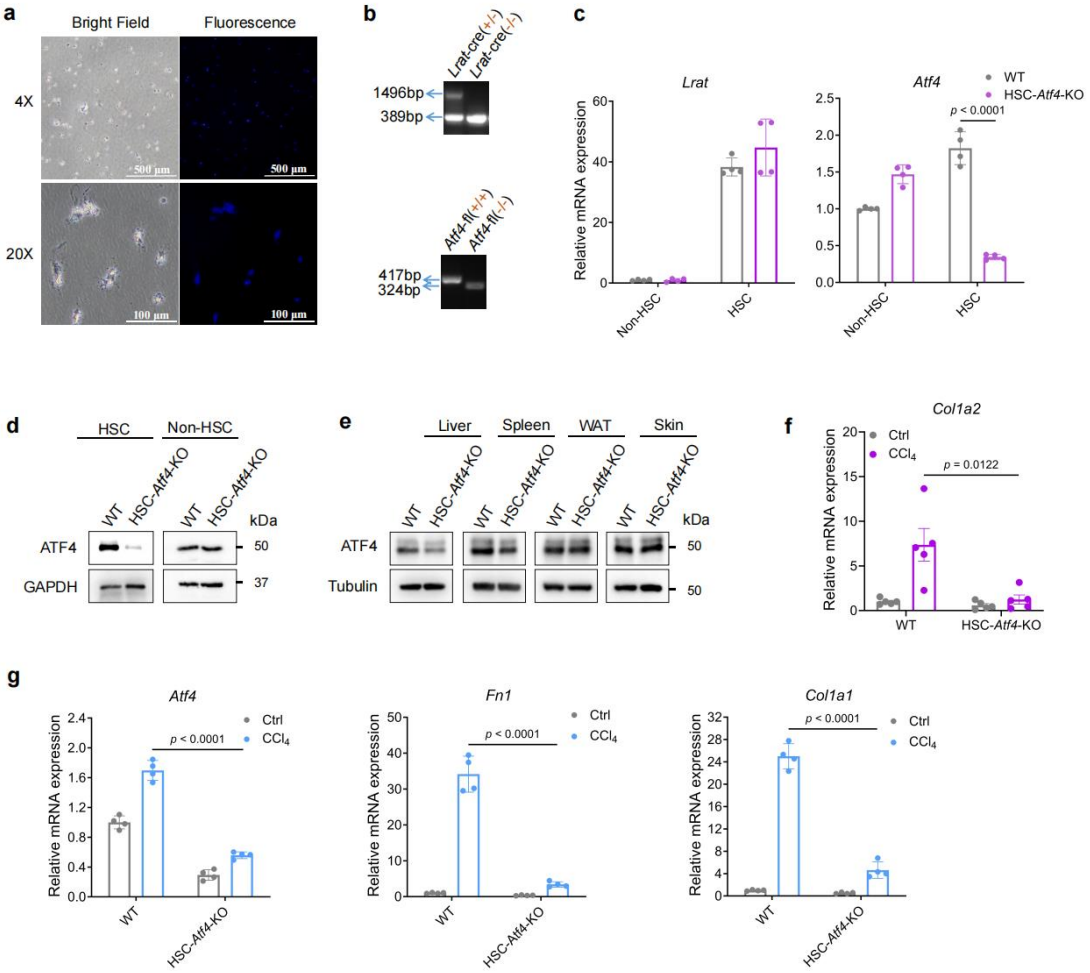

Supplementary Fig. 3 Validation of depletion of ATF4 in the HSC-specific Atf4 knockout mice. a, Representative images showing cell morphology and lipid droplets in isolated HSCs under a phase-contrast microscope (selected from 3 biological replicates for each group). **b**, Representative DNA electrophoresis of the PCR products from a genotyping experiment. The experiment was repeated three times. **c**, qPCR analysis of Lrat and Atf4 mRNA expression in HSCs and non-HSCs isolated from WT and HSC-Atf4-KO mice (n = 4 samples per group). **d**, Western blots showing the expression of ATF4 in HSCs and non-HSCs isolated from WT and HSC-Atf4-KO mice. The experiment was repeated three times. **e**, Western blots showing the expression of ATF4 in four tissues, including liver, spleen, white adipose tissue (WAT), and skin, isolated from WT and HSC-Atf4-KO mice. The experiment was repeated three times. **f**, qPCR analysis showing the expression of Col1a2 in the liver tissues of WT and HSC-Atf4-KO mice treated with or without CCl4 (n = 5 samples per group). **g**, qPCR analysis showing the expression of Atf4, Fn1, and Col1a1 in HSCs isolated from the liver tissues of WT and HSC-Atf4-KO mice treated with or without CCl4 (n = 4 samples per group). Data are presented as mean ± s.e.m. Unpaired, two-tailed Student's t-tests were applied for c, f, and g. ***$p < 0.001$; **$p < 0.01$; *$p < 0.05$. Source data are provided as a Source Data file.

Supplementary Fig. 4

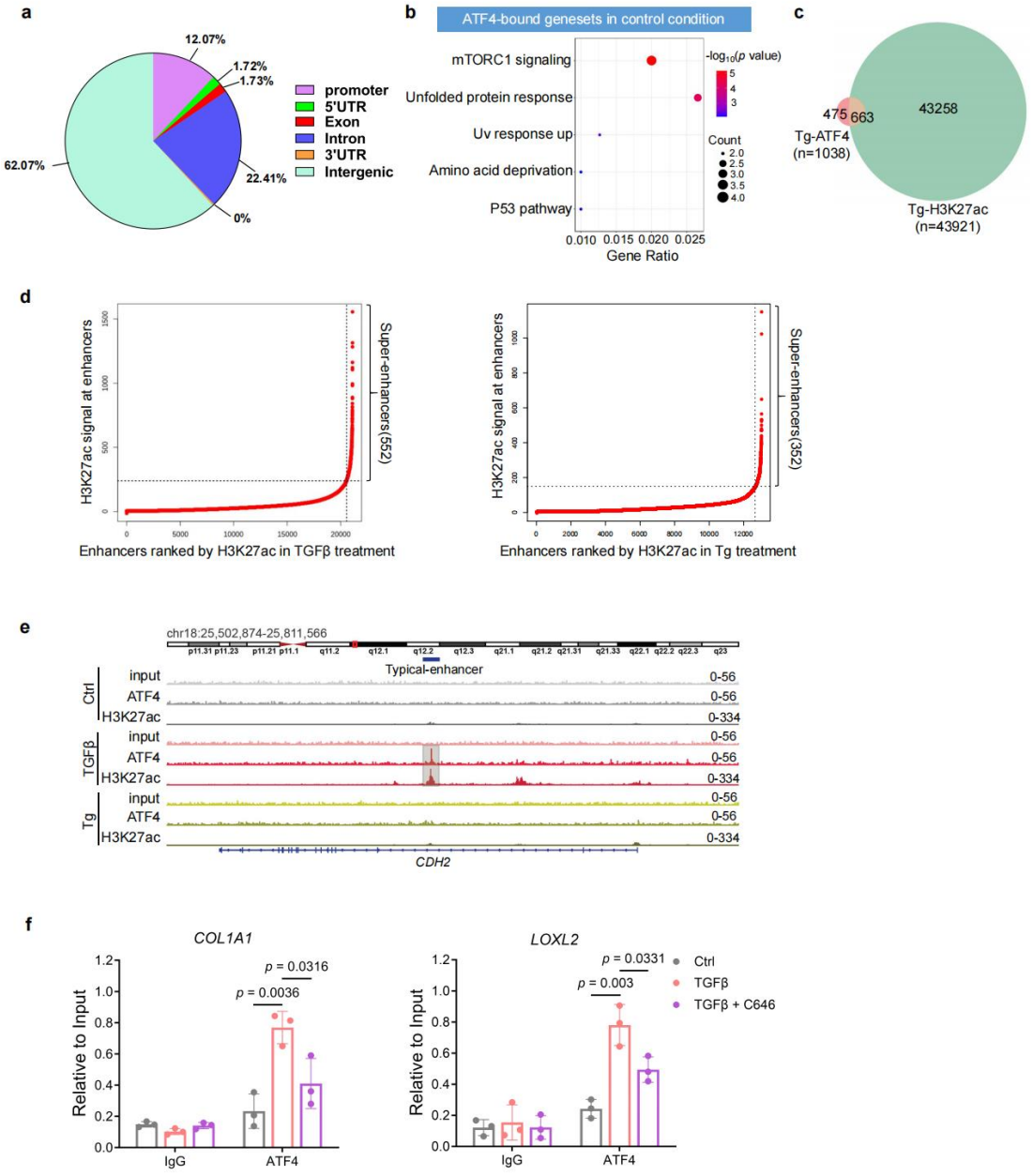

Supplementary Fig. 4 The landscape of ATF4- and H3K27ac- binding regions in different conditions. a, The genome-wide distribution of ATF4 ChIP-seq peaks in the control condition. **b,** GO enrichment analysis for genes that are closest to ATF4 binding sites under control conditions. Top enriched pathways were shown. Hypergeometric test was used to identify significant enrichment pathways ($P < 0.01$). **c,** Venn diagram showing the overlaps between ATF4-bound chromatin regions and H3K27ac-marked chromatin regions under Tg treatment. **d,** Enhancers were ranked by input-subtracted intensity/score of H3K27ac in ER stress and EMT conditions. Super-enhancers (SEs) were determined by the inflection point of the plot. **e,** The snapshots of normalized ATF4, H3K27ac and input ChIP-seq tracks at *CDH2* locus across different conditions: Ctrl, TGFβ, and Tg treatment. The typical enhancers with ATF4 binding sites were highlighted in gray rectangles. **f,** ChIP-qPCR analysis showing the recruitment of ATF4 in the corresponding regions of *COL1A1* and *LOXL2* in the presence of solvent control, TGFβ, or combined TGFβ and C646 (n = 3 biological replicates). Data are presented as mean ± s.e.m. Unpaired, two-tailed Student's t-tests were applied for **f**. ***$p < 0.001$; **$p < 0.01$; *$p < 0.05$. Source data are provided as a Source Data file.

Supplementary Fig. 5

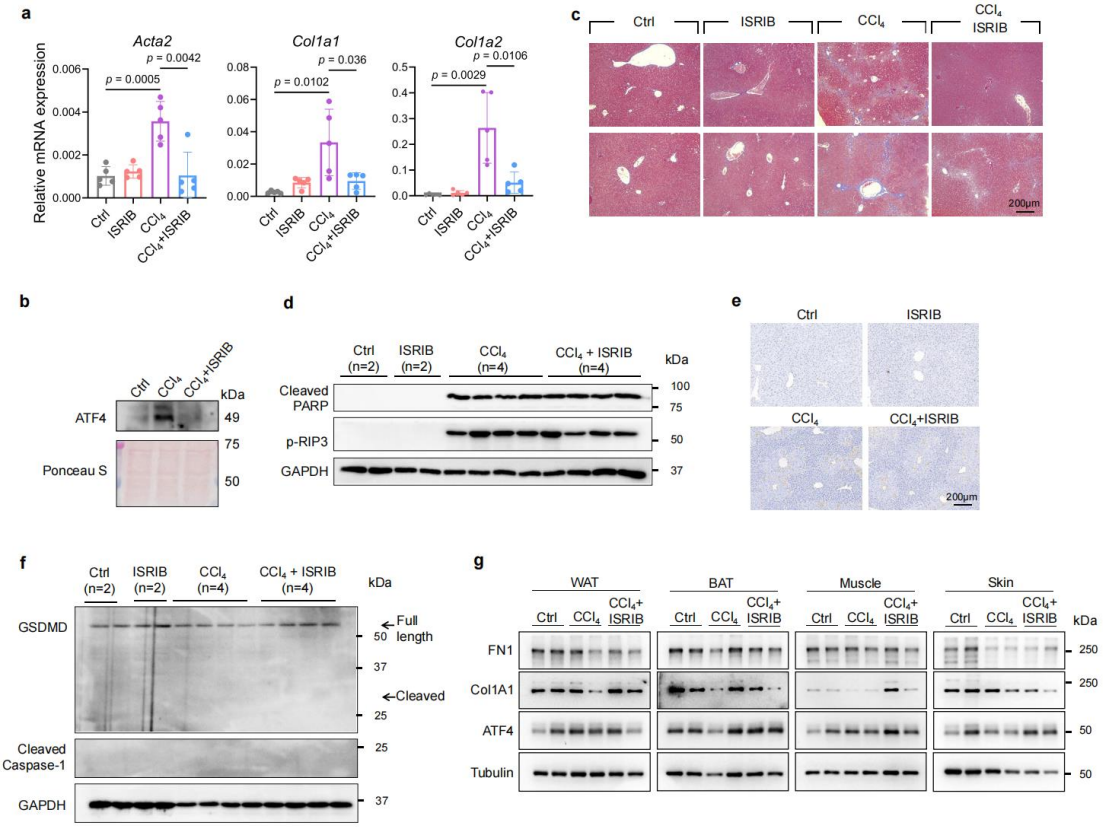

Supplementary Fig. 5 Pharmacological inhibition of eIF2α-ATF4 alleviates CCl_4-induced liver fibrosis. a, 8-week-old male C57BL/6 mice were administrated with CCl_4 (0.5 ml/kg) or solvent control (corn oil) and simultaneously with or without ISRIB (5 mg/kg) twice weekly for 5 weeks. qPCR analysis showing the expression of EMT and fibrotic marker genes in the liver tissues of mice with indicated treatments (n = 5 samples per group). **b,** Western blots showing the expression of ATF4 in HSCs isolated from the liver tissues of mice administrated with corn oil, CCl_4, or CCl_4 combined with ISRIB. The experiment was repeated three times. **c,** The representative images of Masson's trichrome staining for liver tissues of **a** (derived from 3 mouse livers per group). **d,** Western blots showing the expression of cleaved PARP and phosphorylated RIP3 in the liver tissues collected from animals treated with indicated reagents for 24 hr. The experiment was repeated three times. **e,** Representative images from TUNEL staining for livers collected from **d** (derived from 3 mouse livers per group). **f,** Western blots showing the expression of GSDMD and cleaved Caspase-1 in the liver tissues collected from **d**. The experiment was repeated three times. **g**, Western blots showing the expression of ATF4 pathway genes in the indicated tissues collected from animals of **a**. The experiment was repeated three times. Data are presented as mean ± s.e.m. Unpaired, two-tailed Student's t-tests were applied for **a**. ***$p < 0.001$; **$p < 0.01$; *$p < 0.05$. Source data are provided as a Source Data file.

Supplementary Fig. 6

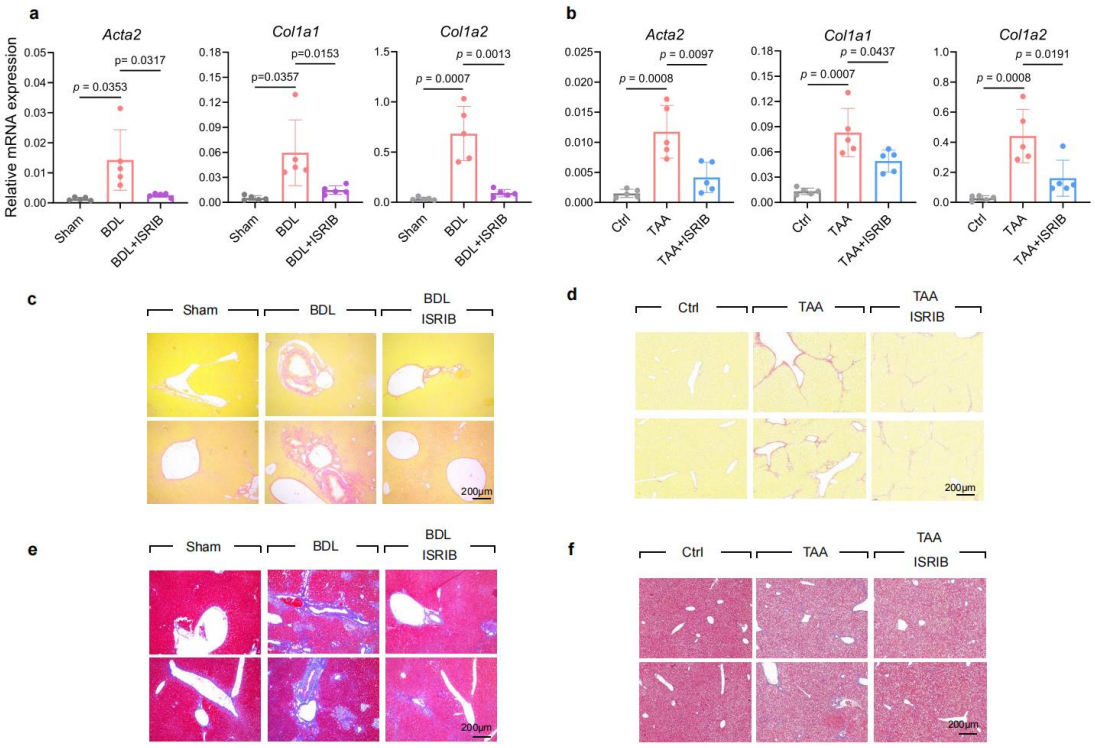

Supplementary Fig. 6 Pharmacological inhibition of eIF2α-ATF4 alleviates BDL- or TAA-induced liver fibrosis. a, qPCR analysis of EMT and fibrotic marker genes expression in livers from mice operated with or without common bile duct ligation and administrated with or without ISRIB (n = 5 samples per group). **b,** qPCR analysis of EMT and fibrotic marker genes expression in livers from mice treated with solvent control, TAA, or a combination of TAA and ISRIB (n = 5 samples per group). **c,** The representative images of Sirius red staining for liver tissues of **a** (derived from 3 mouse livers per group). **d,** The representative images of Sirius red staining for liver tissues of **b** (derived from 3 mouse livers per group). **e,** The representative images of Masson's trichrome staining for liver tissues of **a** (derived from 3 mouse livers per group). **f,** The representative images of Masson's trichrome staining for liver tissues of **b** (derived from 3 mouse livers per group). Data are presented as mean ± s.e.m. Unpaired, two-tailed Student's t-tests were applied for **a, b**. ***$p < 0.001$; **$p < 0.01$; *$p < 0.05$. Source data are provided as a Source Data file.

Supplementary Fig. 7

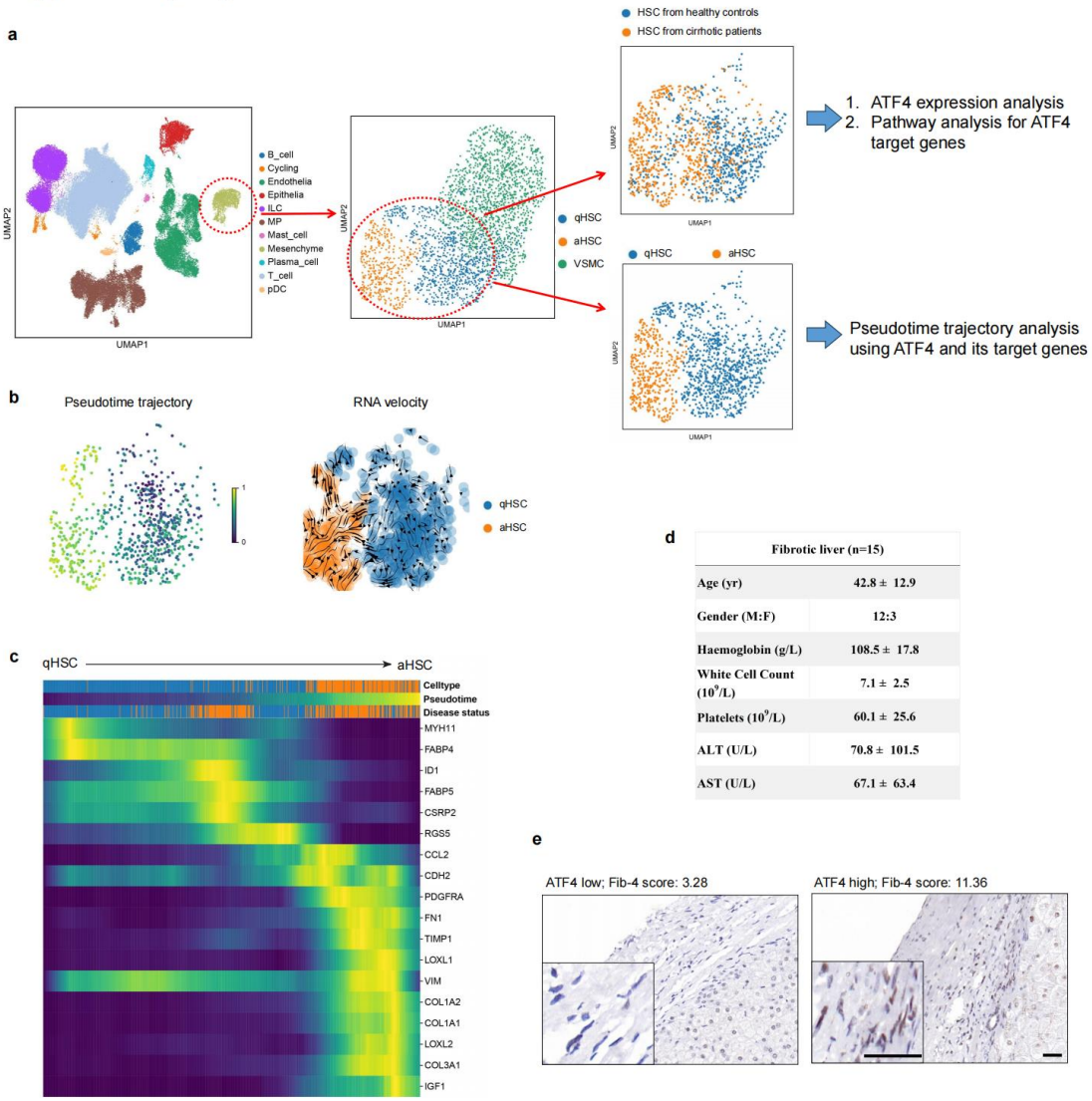

d

Fibrotic liver (n=15)	
Age (yr)	42.8 ± 12.9
Gender (M:F)	12:3
Haemoglobin (g/L)	108.5 ± 17.8
White Cell Count (10^9/L)	7.1 ± 2.5
Platelets (10^9/L)	60.1 ± 25.6
ALT (U/L)	70.8 ± 101.5
AST (U/L)	67.1 ± 63.4

Supplementary Fig. 7 Clinical relevance of HSC-ATF4 in human liver fibrosis. a, UMAP embedding of scRNA-seq data showing 81,714 cells including 11 major cell types (B cell; Cycling; Endothelia; Epithelia; ILC: Innate lymphoid cell; MP: Mononuclear phagocyte; Mast cell; Mesenchyme; Plasma cell; T cell; pDC: Plasmacytoid dendritic cell) from healthy (n = 5) and cirrhotic (n = 5) human livers in the left panel; UMAP embedding of scRNA-seq data showing 2,715 mesenchymal cells annotated by subtypes (qHSC: quiescent HSC; aHSC: activated HSC; VSMC: vascular smooth muscle cells) in the middle panel; UMAP embedding for HSCs stratified by sample source (upper) or activation status of HSC (lower) in the right panel. **b,** UMAP embedding of scRNA-seq data for the pseudo-time trajectory of qHSC and aHSC subclusters (left panel). Close-up of the UMAP embedding colored by qHSC and aHSC subtypes. Arrows indicate overlaid RNA velocity streamlines showing the cell-state transitions inferred by scVelo's dynamical mode from the displayed cells (right panel). **c,** Heatmap showing dynamically expressed genes ordered according to the predicted pseudotime that illustrated the waves of gene expression underlying transition from qHSC to aHSC. **d,** clinical features of patients whose liver tissues were used for ATF4 staining. **e,** Two representative images of IHC staining for ATF4 in fibrotic liver tissues, along with the Fib-4 scores of the patients. Scale bar: 30 μm.

SUPPLEMENTARY TABLES

Supplementary Table 1. Sequences of quantitative PCR primers.

Gene	Primer sequences (5'-3')
ATF4	F: 5'-CTTGATGTCCCCCTTCGACC-3'
	R: 5'-GAAGGCATCCTCCTTGCTGT-3'
ACAT2	F: 5'-TTCATCGGGATGGAGTCTGCTGG-3'
	R: 5'-TCGGTCGGCAATGCCAGGGT-3'
COL1A1	F: 5'-TGATGGGATTCCCTGGACCT-3’
	R: 5'-GGGCCTTGTTCACCTCTCTC-3'
COL1A2	F: 5'-TGGTCTCGGTGGGAACTTTG-3’
	R: 5'-CACCCTGTGGTCCAACAACT-3’
FN1	F: 5'-CAGTGGGAGACCTCGAGAAG-3’
	R: 5'-TCCCTCGGAACATCAGAAAC-3'
CDH2	F: 5'-ACAGTGGCCACCTACAAAGG-3’
	R: 5'-CCGAGATGGGGTTGATAATG-3’
VIM	F: 5'-GAGAACTTTGCCGTTGAAGC-3’
	R: 5'-GCTTCCTGTAGGTGGCAATC-3’

SNAI1	F: 5'-CTGCAGGACTCTAATCCAGAGTTTA-3’
	R: 5-CCACTGTCCTCATCTGACAGG-3'
SNAI2	F: 5'-GGGGAGAAGCCTTTTTCTTG-3’
	R: 5'-TCCTCATGTTTGTGCAGGAG-3'
Atf4	F: 5'-CCTATAAAGGCTTGCGGCCA-3’
	R: 5'-GATTTCGTGAAGAGCGCCAT-3’
Fn1	F: 5'-GGCCACCATTACTGGTCTGG-3’
	R: 5'-GGAAGGGTAACCAGTTGGGG-3’
Acta2	F: 5'-CTTCGTGACTACTGCCGAGC-3'
	R: 5'-AGGTGGTTTCGTGGATGCC-3’
Col1a1	F: 5'-CGATGGATTCCCGTTCGAGT-3'
	R: 5'-CGATCTCGTTGGATCCCTGG-3'
Col1a2	F: 5'-CCAAGGGTGCTACTGGACTC-3’
	R: 5'-TTTCCTTCTTCACCGCTGGG-3'

Supplementary Table 2.Sequences of primers used for plasmid construction.

Inserted DNA	Primer Sequence (5’-3')
pGL3-COL1A1-enhancer	F: 5'-GAGCTCTTACGCGTGCACGTGGCCTCCCCCTTTTCTGC-3' R: 5'-AGATCTCGAGCCCGGGCTGGCCTGGGGAGAGCAGCTGT-3'
shATF4-1#	F: 5'-CCGGCCACTCCAGATCATTCCTTTACTCGAGTAAGGAATGATCTGGAGTGGTTTTTG-3' R: 5'-AATTCAAAAACCACTCCAGATCATTCCTTTACTCGAGTAAAGGAATGATCTGGAGTGG-3’
shATF4-2#	F: 5'-CCGGGCCTAGGTCTCTTAGATGATTCTCGAGAATCATCTAAGAGACCTAGGCTTTTTG-3' R: 5'-AATTCAAAAAGCCTAGGTCTCTTAGATGATTCTCGAGAATCATCTAAGAGACCTAGGC-3'
shATF4-3#	F: 5'-CCGGCATGATCCCTCAGTGCATAAACTCGAGTTTATGCACTGAGGGATCATGTTTTTG-3' R: 5'-AATTCAAAAACATGATCCCTCAGTGCATAAACTCGAGTTTATGCACTGAGGGATCATG-3'